IEEE Open Journal of
Antennas and Propagation

Received 24 December 2022; revised 18 January 2023; accepted 22 January 2023. Date of publication 30 January 2023; date of current version 10 February 2023.

Digital Object Identifier 10.1109/OJAP.2023.3240850

Beamwidth Enhancement of Microstrip Antennas Using Capacitive Via-Fence Loading

ZHENYU LIU [1], YIJING HE [2] (Member, IEEE), AND YUE LI [1] (Senior Member, IEEE)

[1]Department of Electronic Engineering, Tsinghua University, Beijing 100084, China

[2]School of Integrated Circuits and Electronics, Beijing Institute of Technology, Beijing 100081, China

CORRESPONDING AUTHOR: Y. LI (e-mail: lyee@tsinghua.edu.cn)

This work was supported in part by the National Natural Science Foundation of China under Grant 62022045 and Grant U22B2016, and in part by the Shenzhen Science and Technology Program under Grant JSGG20210802153800002.

ABSTRACT In this paper, a general approach to enhance the beamwidth of microstrip antennas is proposed for wide beam coverage in both E- and H-planes. A microstrip antenna loaded with two arrays of capacitive via fences is propounded and systematically studied. By introducing the vertical currents brought by the capacitive metalized vias, the half-power beamwidth (HPBW) is effectively broadened compared with the regular microstrip antennas. In addition, by utilizing the air medium with low loss, the microstrip antenna can be supported by the two arrays of via fences, maintaining a high radiation efficiency. To validate the proposed design, a prototype is fabricated and tested. The measurement results agree well with the simulated ones, with enhanced HPBWs of 100° and 90° in E- and H-planes, respectively. Compared with the existing 2.4-GHz antennas, the propounded antenna is with the advantages of wide beamwidth and high radiation efficiency, exhibiting the potential applications for space-limited mobile devices with wide coverage requirement.

INDEX TERMS Microstrip antenna, half-power beamwidth, metalized blind vias, antenna radiation efficiency.

I. INTRODUCTION

DUE TO the benefits of simple fabrication process and easy integration, microstrip antennas are widely utilized in the applications of communications [1], [2], [3], sensing [4], and RF harvesting [5]. By engineering various advanced structures, microstrip antennas have successfully achieved important properties for antennas, such as broad bandwidth [6], [7] and dimension miniaturization [8], [9]. However, for a typical microstrip antenna in a mobile device, the E- and H-planes' HPBWs is usually less than 80°, limiting the applications of wide beam coverage. What's more, with the variation of the ground sizes of different mobile devices, the beamwidth also undergoes drastic reduction. Therefore, a feasible approach to enhance the beamwidth is required for microstrip antennas in mobile devices for wide beam coverage.

Different antenna design methods are developed to realize the wide beam coverage [10], [11], [12], [13], [14], [15], [16], [17], [18], and can be divided into five categories. The first one utilizes a thick substrate on the antennas [19], [20]. Two typical way of utilizing thick profile is by designing dielectric resonator antenna (DRA) and magnetoelectric dipole antenna. In [21], the authors utilize a dielectric resonator antenna (DRA) with an engraved groove and a comb-like metal wall for beamwidth enhancement in both E- and H-planes. In [22], the authors design a dual-polarized magnetoelectric dipole antenna with gain improvement at low elevation angle for a base station. In this way, by enhancing the radiation of low elevation, the beamwidth is effectively broadened [23], [24], [25]. In addition, by utilizing the thick profile, the bandwidth is enhanced at the same time. However, a thick profile will bring some effect to the antenna performance, such as an increase in antenna loss and a decrease in radiation efficiency. The second approach is to reshape the ground plane of the antenna, such as reducing the size of the ground plane [26], [27], [28]

and introducing a 3-D ground plane under the patch [26], [29]. The beamwidth of the antenna can be broadened by making the floor edge current participate in the radiation. Accordingly, reducing the size of the ground leads to a front-to-back ratio less than 10 dB by introducing the strong back lobe. This approach is simple and convenient, but some application scenarios do not allow changing the size of the ground plane. The third method broadens the HPBW by reducing the size of the antenna [30], [31], [32]. By reducing the distance of two radiation apertures of the antenna, the broadside gain is decreased and the HPBW is broadened. This method can reduce the cost and size occupied by the antenna. However, reducing the size of the antenna will result in a reduction in bandwidth and efficiency. The fourth way to achieve beamwidth enhancement is by adopting parasitic structures around the main radiator [33], [34], [35], [36], [37]. The parasitic structure can effectively compensate for the radiation but makes the whole structure too large to use. In the fifth approach, surface waves can be excited via the introduction of a loaded high dielectric constant material to broaden the beamwidth [25]. However, utilizing a high dielectric constant medium usually lead to a narrow bandwidth which limits the application of antennas.

For traditional microstrip antennas, with the change in the ground size of smart devices, the beamwidth will undergo a drastic change and deterioration. Here, to solve this problem, we proposed a general method to achieve the beamwidth enhancement of microstrip antenna using capacitive via-fence loading to compensate the ground effect. In this way, we can achieve the optimal beamwidth with a certain size of the ground plane. By applying the vertical current introduced by the metalized blind vias, the radiation pattern at low elevation angles can be compensated thus broadening the beamwidth. In this way, the beamwidth of the antenna is effectively enhanced without the occupation of large space and the decrease in bandwidth and efficiency. In addition, the overall antenna size is obviously reduced due to the capacitive loading effect introduced by blind vias. Furthermore, by employing the low loss air medium the total efficiency exceed 88% in the operating range of 2.39∼2.49 GHz to fulfill the requirement for high-speed and low-latency communication.

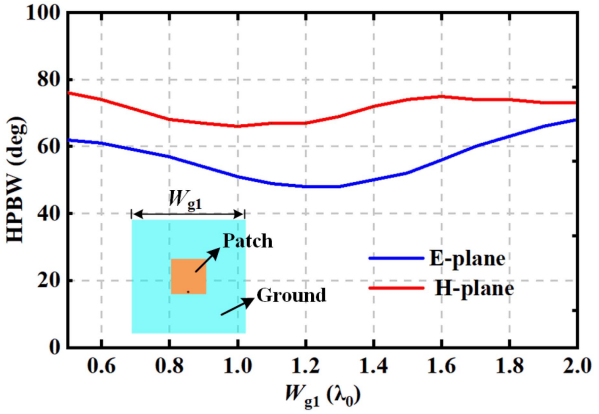

FIGURE 1. Simulation values of the E- and H-planes' HPBWs of the normal microstrip antenna with different W_{g1}.

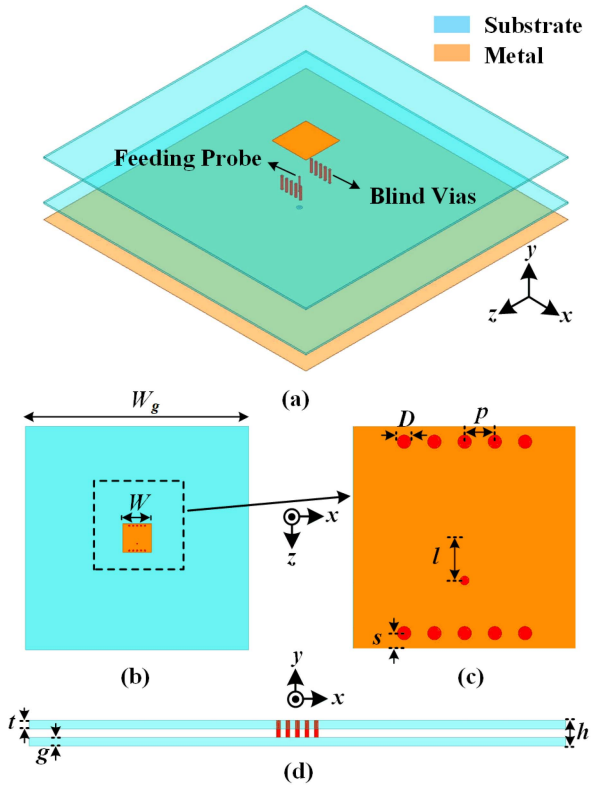

FIGURE 2. (a) Exploded view, (b) top view, (c) detailed view, and (d) cross-sectional view of the proposed antenna.

II. ANTENNA DESIGN

A. ANTENNA GEOMETRY AND STRUCTURE

As illustrated in Fig. 1, we first discuss the influence of ground size on the beamwidth of a normal microstrip antenna. We assume a microstrip antenna operated at 2.44 GHz, which is the center frequency of the Wireless Local Area Networks (WLAN) band, and λ_0 is the free-space wavelength at 2.44 GHz. $\boldsymbol{W_{g1}}$ is the ground size of the microstrip antenna. From Fig. 1, we can figure out that the ground size affects the HPBWs of both the E- and H-planes of the microstrip antenna, and the E-plane HPBW is less than 60° under most ground sizes and the beamwidth is too narrow to use. Our goal is to find a way to broaden the beamwidth of both the E- and H-planes. Without the loss of generality, we choose a common and widely used ground size of 1.5 λ_0 to present our design. The geometric views of the propounded antenna are depicted in Fig. 2. The propounded antenna consists of a radiation patch, metalized blind via fences, two dielectric substrates, and a metal ground plane. An F4BM dielectric substrate with a permittivity of 2.65 and a loss tangent of 0.002 is used to manufacture the metalized patch. The blind vias are with diameter ($\boldsymbol{D}$), period ($\boldsymbol{p}$), and gap ($\boldsymbol{g}$) to metallic ground. They are connected on both sides of the radiating apertures. There is no difference

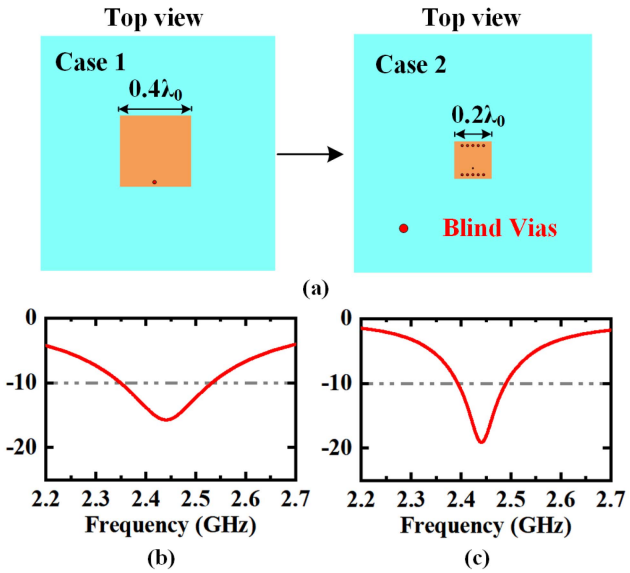

FIGURE 3. (a) Evolution of the proposed method. Simulated S_{11} of (b) Case 1 and (c) Case 2.

TABLE 1. Detailed dimensions in Figure 2.

Parameter	Value (mm)	Parameter	Value (mm)	Parameter	Value (mm)
W_g	187.5	P	3.3	g	1.0
W	24.3	l	4.7	t	1.0
D	1.5	s	1.7	h	9.0

in size between these blind vias and the holes in the upper substrate. The printed ground is 2 mm thick on the back of the dielectric that supports the structure. Fig. 2(b) shows the metalized patch at the top and two substrates as squares with $\boldsymbol{W}$ and $\boldsymbol{W_g}$ side lengths. In Fig. 2(c), the antenna is shown from a cross-section view. For simplicity, the bottommost substrate is made from the same F4BM material as the upper one. A 50-Ω semi-grid cable is utilized to feed the antenna, with the inner and outer conductors soldered to the top patch and bottom metallic ground. Table 1 provides specific geometrical parameters of the proposed design. Here, Ansoft High Frequency Structure Simulator (HFSS) is used to optimize the antenna.

To clarify the evolution of the propounded approach, Fig. 3 illustrates the comparison of the sizes and S_{11} of the two cases of the regular microstrip antenna and the proposed antenna with two arrays of via fence. The two cases are with the same center operating frequency (2.44 GHz), the same ground size (1.5 $\lambda_0 \times 1.5\ \lambda_0$), and profile (0.07 λ_0), where λ_0 is the free-space wavelength at the 2.44 GHz. Clearly, via applying the propounded blind vias onto the two radiation apertures of the patch antenna, the size of the patch is obviously miniaturized from 0.4 $\lambda_0 \times 0.4\ \lambda_0$ to 0.2 $\lambda_0 \times 0.2\ \lambda_0$. Accordingly, the bandwidth of the antenna is reduced from 180 MHz (2.35-2.53 GHz) to 100 MHz (2.39- 2.49 GHz). Figs. 4 and 5 illustrated the simulated 3-D radiation pattern of Case 1 and Case 2, respectively. It is obvious that

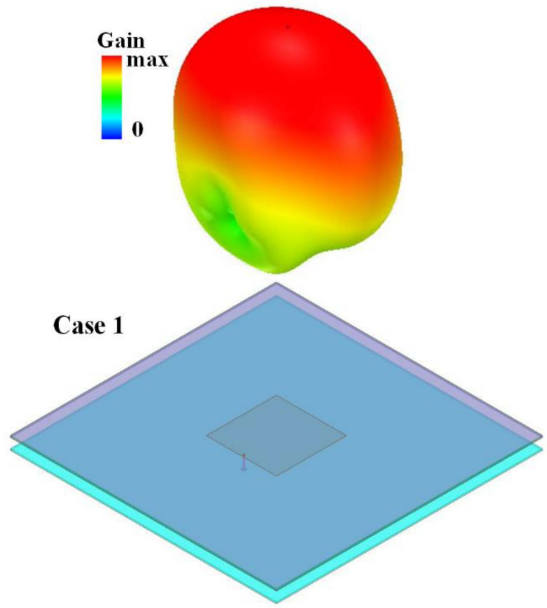

FIGURE 4. Simulated 3-D radiation pattern of Case 1.

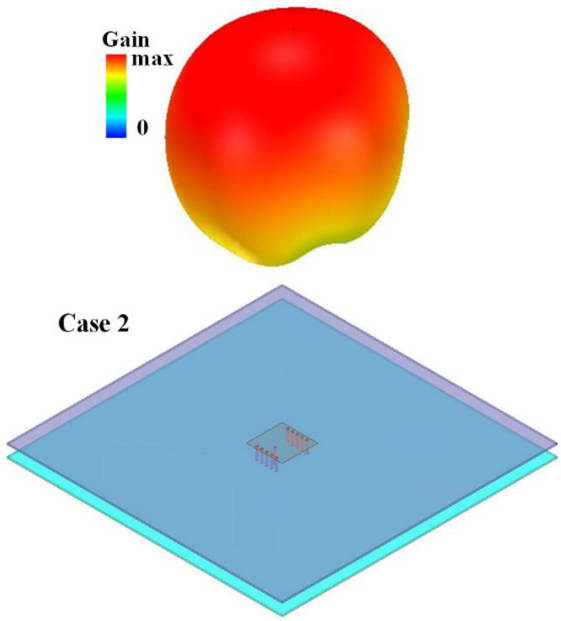

FIGURE 5. Simulated 3-D radiation pattern of Case 2.

compared with Case 1,the coverage area of Case 2 in the upper half plane has improved significantly. To be more specific, Fig. 6 depicts a comparison of the normalized E-plane radiation pattern of Case 1 and Case 2. It is clear that by applying the capacitive blind vias at the radiating aperture of a normal microstrip antenna, we not only double the E-plane HPBW from 52° to 101° but also broaden the H-plane HPBW from 74° to 91°. It is worth noticing that once applying the capacitive via-fence, the E-plane radiation pattern becomes unsymmetrical. To explain this phenomenon, Fig. 7 depicts the complex E-field magnitude distribution

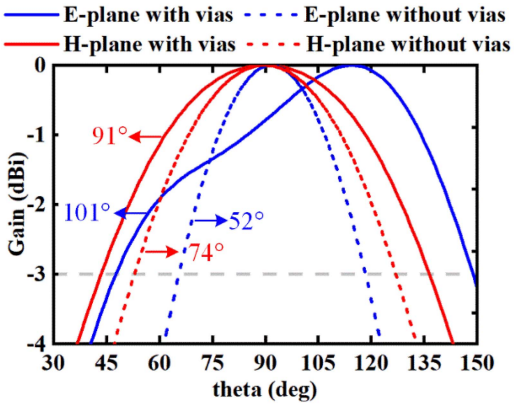

FIGURE 6. Comparison of E- and H-planes normalized radiation pattern of with blind vias (Case 2) and without blind vias (Case 1).

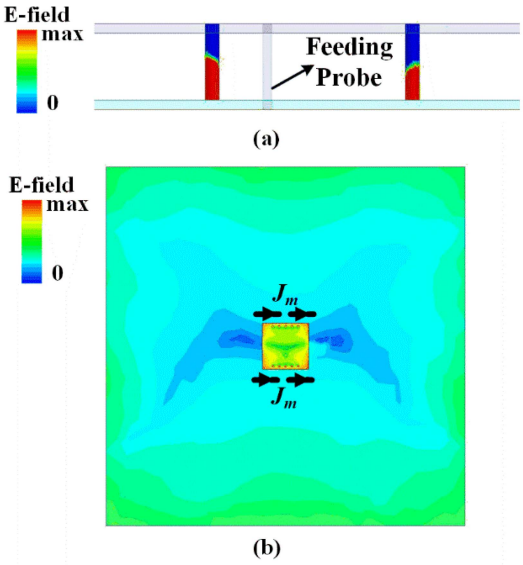

FIGURE 7. Complex E-field magnitude distribution on the (a) the blind vias and (b) the patch and the ground plane.

of the blind vias, the patch, and the ground plane. From Fig. 7(a), it is clear that the electric field magnitude on the two sides of the blind vias is not the same. The electric field strength is stronger on the blind vias which are closer to the feeding probe. In this way, the radiation pattern generated by the two sides of the blind vias is asymmetric. From Fig. 7(b), we can see that loading the blind vias will not affect the TM_{10} mode of the patch antenna. Based on Huygen's principle, two magnetic currents lined up with a distance of $\boldsymbol{d}$ can approximately represent the radiation property of the antenna. Based on these two equivalent magnetic currents, the proposed antenna is able to achieve a broadside radiation pattern.

B. PRINCIPLE OF BEAMWIDTH ENHANCEMENT

Next, we discuss the principle of beamwidth enhancement of the proposed method. First, as we demonstrated above, the radiation of the patch antenna is equivalent to the radiation of two magnetic currents at the aperture. Therefore, the two

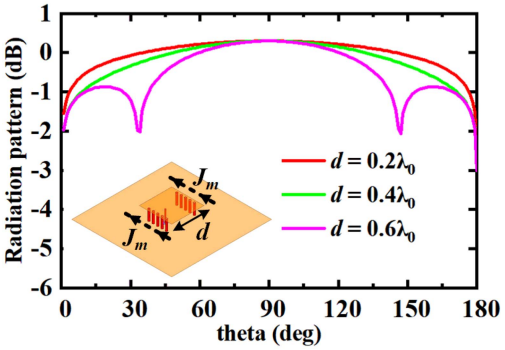

FIGURE 8. Simulated radiation pattern of array factor (AF) when d is $0.2\lambda_0$, $0.4\lambda_0$ and $0.6\lambda_0$.

in-phase magnetic currents construct a two-element array that can represent the radiation property of the patch. As we know, the radiation pattern of the array is equal to the product of the element factor and array factor. The array factor is given as $2\cos(\pi d\cos\theta)$, where $\boldsymbol{d}$ is the electrical length of the two magnetic currents and θ is the pitch angle between the z-axis and x-axis. We then assume the broadside radiation element factor as $\sin\theta$, so the radiation pattern of the proposed method can be written as $2\sin\theta\cos(\pi d\cos\theta)$. Therefore, we can figure that the distance between the two magnetic currentsaffects the radiation pattern and the beamwidth. In order to analyze the extent to which the distance between the two magnetic currents affects the beamwidth, here we plot the ideal radiation pattern in log format as Fig. 8. From Fig. 8, we can clearly see that when $\boldsymbol{d}$ varies from 0.2 λ_0 to 0.4 λ_0, the radiation pattern and beamwidth only have a slide change. In contrast, when $\boldsymbol{d}$ switch from 0.4 λ_0 to 0.6 λ_0, the radiation pattern show some obvious changes, such as the emergence of the sidelobe and dramatic deterioration of beamwidth Therefore, as illustrated in Fig. 8, we can conclude that from Case 1 to Case 2, the narrowing of current distance indeed has an effect on the enhancement of the beamwidth, but it is obviously not the dominant reason for that. As shown in Fig. 9(a), the current distributions on the proposed antenna are comprised of two parts: the horizontal current $\boldsymbol{J_h}$ and the vertical current $\boldsymbol{J_v}$. The horizontal current is generated on the radiating patch, which forms a narrow beam radiation pattern with unidirectional radiation. Besides, the vertical current is generated on the blind vias, which forms a radiation pattern with ∞-shape. According to the superposition theorem of patterns, the radiation of the antenna at the low elevation angles is increased. Therefore, the beamwidth of the proposed microstrip antenna is broadened evidently. It is concluded that both reducing the distance of equivalent magnetic current and introducing the vertical current can broaden the beamwidth but the dominant factor for broadening beamwidth is the second one.

C. PARAMETER DISCUSSION

Next, some essential parameters of the propounded antenna are further discussed. Fig. 10 and Fig. 11 show the simulation E- and H-planes normalized radiation pattern with

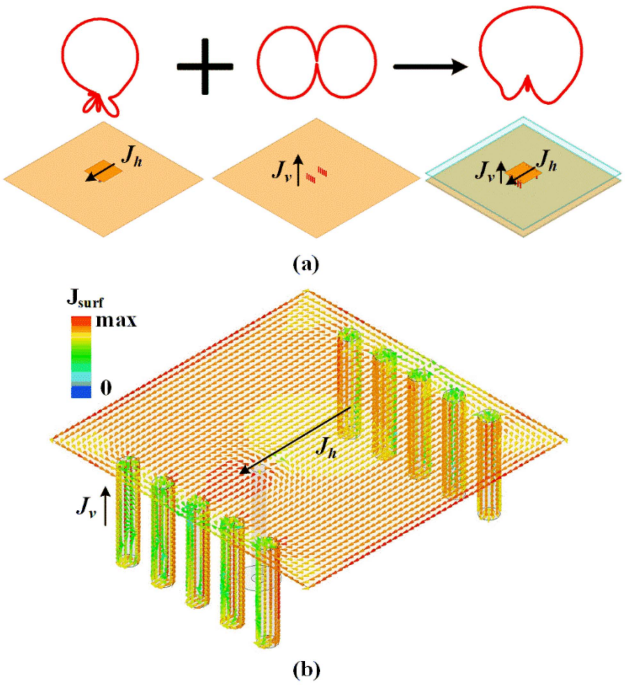

FIGURE 9. (a) Principle of the beamwidth enhancement of the proposed antenna. (b) Vector surface current distribution of the proposed structure.

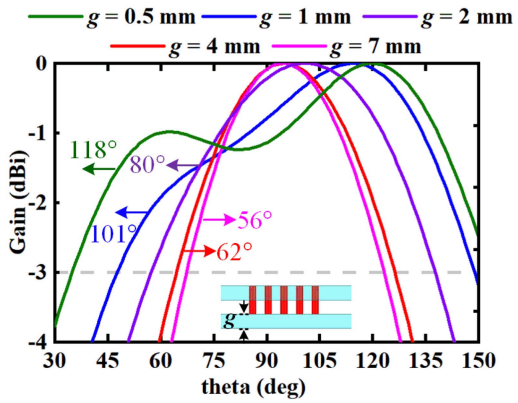

FIGURE 10. Comparison of the E-plane normalized radiation pattern with various gap (*g*).

various gaps (***g***). It can be seen that in either the E- and H-planes, the HPBW is getting larger when the gap gets smaller. As the ***g*** changes from 7 mm to 0.5 mm, the E- and H-planes' HPBWs are raised from 51° to 118° and 76° to 96°, respectively. The reason for this pattern is that the smaller the gap brings the larger the capacitance of the blind vias, which results in a larger vertical current appearing on the blind vias. As we have demonstrated, the generation of vertical current is the key to the beamwidth enhancement effect of the proposed method. What's more, the smaller the gap, the more asymmetric the electric field magnitude on the blind vias on the two sides. Thus reducing the gap will make the E-plane pattern asymmetric. According to the

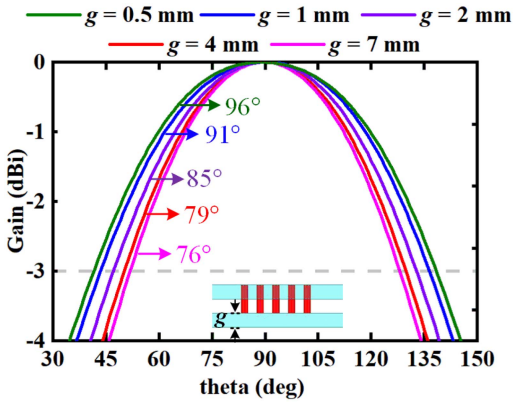

FIGURE 11. Comparison of H-plane normalized radiation pattern with various gap (*g*).

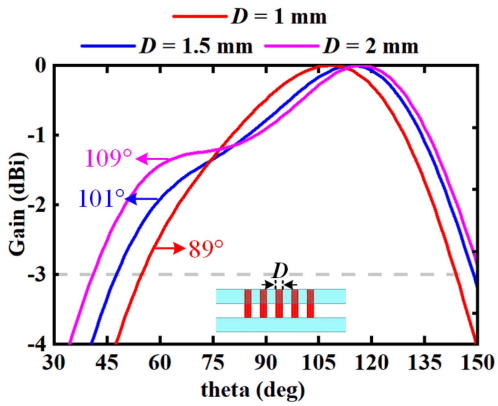

FIGURE 12. Comparison of E-plane normalized radiation pattern with various diameter (*D*).

conclusion in [38], the minor gap will bring a narrower bandwidth and the case of $\boldsymbol{g} = 1$ mm is just enough to cover the bandwidth of 2.4-2.48 GHz. Therefore, in order to maintain the bandwidth and facilitate processing, we at last choose the $\boldsymbol{g} = 1$ mm as the final result. Fig. 12 and Fig. 13 depicts the simulation E- and H-planes normalized pattern with various diameters (***D***). Adjusting diameter ***D*** from 1 mm to 2 mm results in the enhancement of the E- and H-planes' HPBWs from 89° to 109° and 89° to 94°, respectively. Since the greater diameter of blind vias can carry more vertical current on the surface, as a result, a wider beamwidth is produced for both E- and H-planes. Similar to the gap (***g***), greater ***D*** narrows the bandwidth of the proposed antenna, and thus for the same bandwidth consideration, we set ***D*** as 1.5mm. As shown in Fig. 14 and Fig. 15, changing the period (***p***) is only with a minor effect on the radiation of both the E- and H-planes.

III. PROTOTYPE AND MEASUREMENT RESULTS

Validation has been accomplished through the fabrication and testing of a prototype. The antenna is fed from a semi-grid cable as shown in Fig. 16. According to Fig. 17, the measured S_{11} is in good agreement with the simulation results obtained with the N9917A vector network

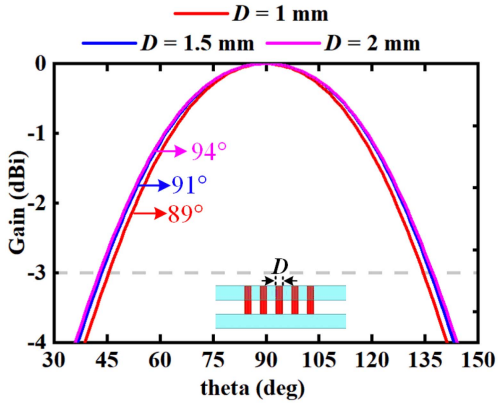

FIGURE 13. Comparison of H-plane normalized radiation pattern with various diameter (*D*).

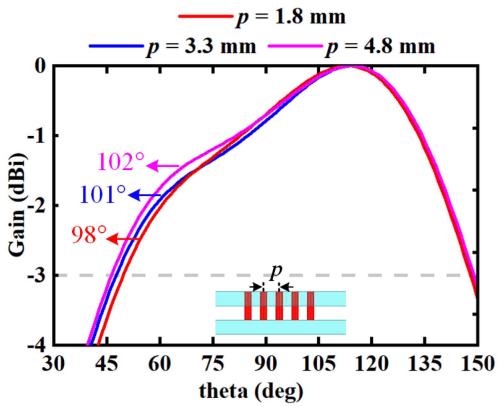

FIGURE 14. Comparison of E-plane normalized radiation pattern with various period (*p*).

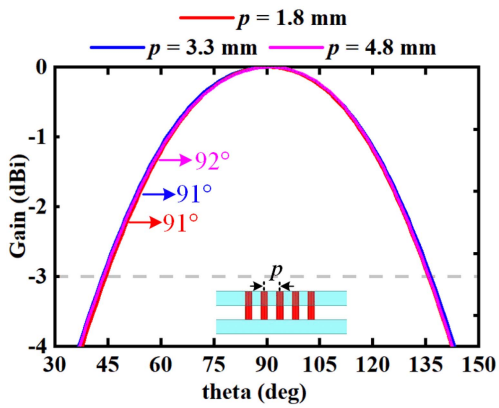

FIGURE 15. Comparison of H-plane normalized radiation pattern with various period (*p*).

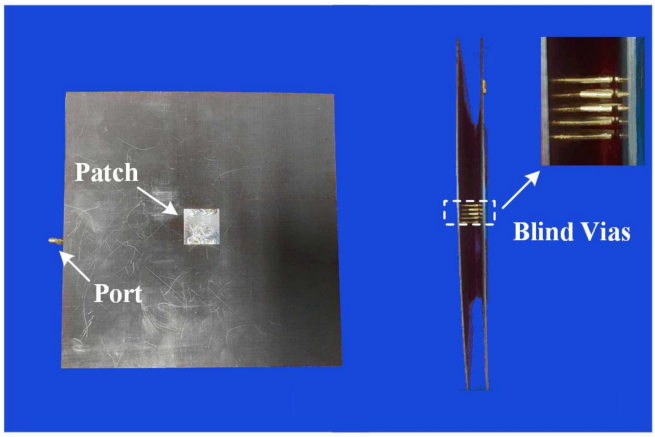

FIGURE 16. Photograph of top view and cross-section views of fabricated prototype.

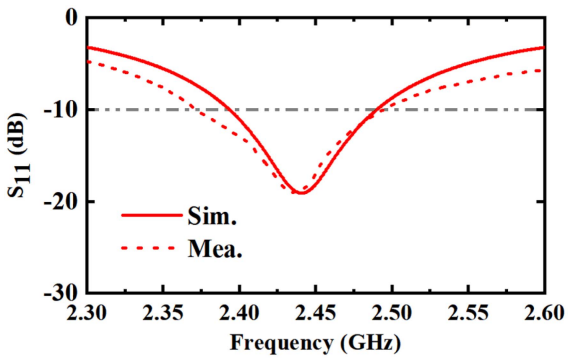

FIGURE 17. Simulated and measured S_{11} of the proposed antenna.

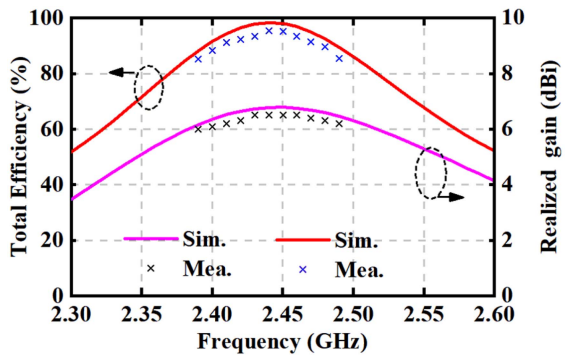

FIGURE 18. Simulated and measured gain and total efficiency of the proposed antenna.

analyzer. The simulation S_{11} is lower than -10 dB from 2.39 GHz to 2.49 GHz and the measurement S_{11} is lower than -10 dB from 2.37 GHz to 2.49 GHz. The minor variation between simulated and measured results is primarily a result of the processing error. In Fig. 18, the simulation and measurement total efficiency and realized gain are illustrated. The simulation realized gain is exceed 6.3 dBi in the operating band. With the low-loss air cavity, the simulated total efficiency is above 91.5% in the operating range of 2.4∼2.48 GHz. The measured gain exceeds 6.1 dBi and the total efficiency exceeds 88.3% over the whole frequency range. Fabrication tolerance is mainly responsible for the minor variation between the simulated and measured results. On the basis of simulations and measurements, Fig. 19 illustrates the normalized radiation patterns of the proposed design at 2.44 GHz. As can be seen, the simulated and measured results are in good agreement. The propounded

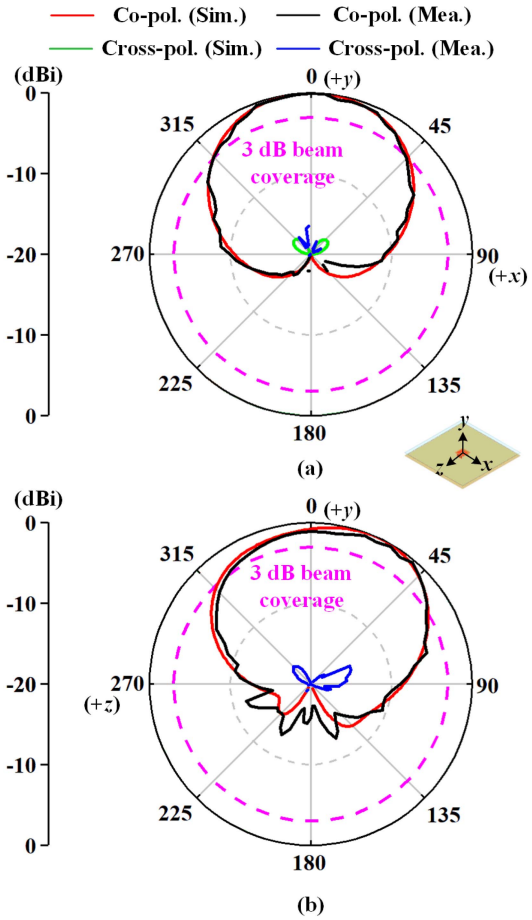

FIGURE 19. Normalized simulated and measured radiation patterns of (a) xoy plane and (b) yoz plane of the proposed antenna at 2.44 GHz.

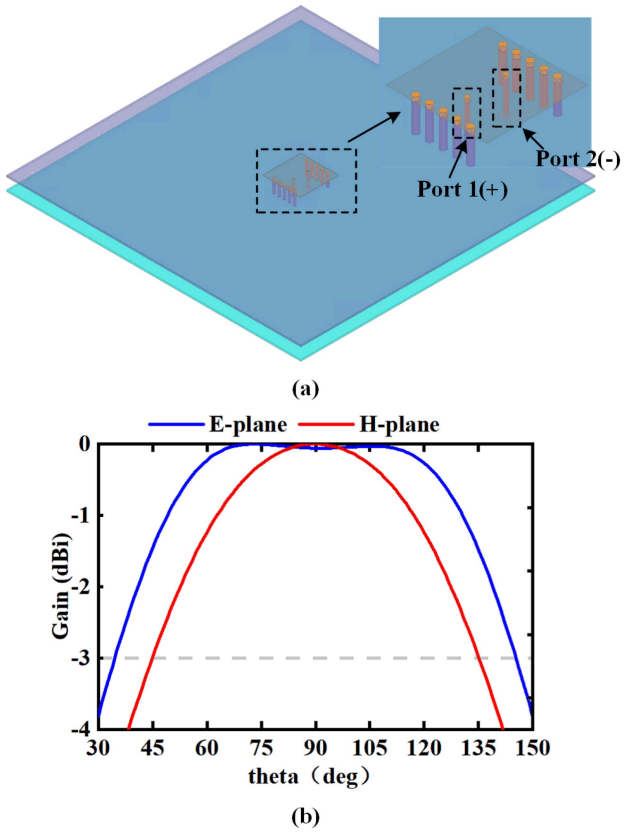

FIGURE 20. (a) Differential feed scheme of the proposed antenna (b) The normalized simulated radiation patterns of E-and H- planes of differential feed scheme antenna at 2.44 GHz.

TABLE 2. Comparison among the proposed design and other related antennas.

Reference	Antenna Type	Size(λ_0^3)	Efficiency	HPBW-E/H(°)
[39]	slot	0.70×1.34×0.21	N.A.	50/60
[40]	patch	0.53×0.50×0.01	40%	50/50
[41]	patch	0.48×0.48×0.06	34%	80/85
[42]	dipole	0.40×0.16×0.14	N.A.	75/70
Proposed	**patch**	**0.20×0.20×0.07**	**88%**	**100/90**

antenna exhibits broadside patterns with a wide beamwidth in both xoy plane (H-plane) and yoz plane (E-plane). The measured xoy plane (E-plane) HPBW reaches 100°, whereas the measured yoz plane (H-plane) HPBW reaches 90°. In addition, as shown in Fig. 19, the simulated and measured front-to-back ratio is greater than 20 dB, exhibiting low back lobes. The difference between the simulated and measured data is primarily caused by the measurement error of feeding cable. As a way of highlighting the ascendency and novelty of the proposed antenna, we draw a table based on antenna type, size, efficiency, and HPBWs of the E- and H-planes. Accordingly, the propounded antenna has a competitive ascendency over the antennas listed in Table 2, including its compact size and wide beamwidth of broadside radiation.

At the end of the paper, we want to add a method to solve the problem of the asymmetry of E-plane radiation pattern by applying the differential feed scheme. As shown in Fig. 20(a), the scheme uses two feeding points with equal amplitude and inverted phase. In this way, as shown in Fig. 20(b), the E-plane radiation pattern can restore to symmetric because the geometric structure becomes symmetric. However, the cost of eliminating the asymmetry of the radiation pattern is to add the differential feed network which will make the structure complicated and lead to the reduction of antenna efficiency. Since the asymmetry of the radiation pattern is normal and does not affect the use of the antenna, we apply the single feed scheme in our manuscript eventually.

IV. CONCLUSION

This paper presents a method to enhance the beamwidth of the microstrip antennas. By utilizing the capacitive via-fence loading, the propounded antenna is with a stronger vertical current which can enhance the radiation of low elevation thus broadening the beamwidth. The approach is validated by fabricating, characterizing, and analyzing a prototype. Over the WLAN band, the measurement results are consistent with the simulation results, manifesting E- and H-planes' HPBWs of 100° and 90°. Thus, the proposed approach has the potential to pave a way for wide coverage and beam scanning.

REFERENCES

[1] L. Sun, Y. Li, and Z. Zhang, "Decoupling between extremely closely-spaced patch antennas by mode cancellation method," *IEEE Trans. Antennas Propag.*, vol. 69. no. 6, pp. 3074–3083, Jun. 2021.

[2] Y. Zhang, Z. Han, S. Shen, C. Chiu, and R. Murch, "Polarization enhancement of microstrip antennas by asymmetric and symmetric grid defected ground structures," *IEEE Open J. Antennas Propag.*, vol. 1, pp. 215–223, 2020.

[3] Y. He and Y. Li, "Compact co-linearly polarized microstrip antenna with fence-strip resonator loading for in-band full-duplex systems," *IEEE Trans. Antennas Propag.*, vol. 119. no. 15, pp. 7125–7133, Nov. 2021.

[4] Y. Hou, Y. Li, L. Chang, Z. Zhang, and Z. Feng, "Bidirectional same-sense circularly polarized antenna using slot-coupled back-to-back patches," *Microw. Opt. Technol. Lett.*, vol. 59, no. 3, pp. 645–648, Mar. 2017.

[5] S. Shen, C. Chiu, and R. Murch, "A dual-port triple-band l-probe microstrip patch rectenna for ambient RF energy harvesting," *IEEE Antennas Wireless Propag. Lett.*, vol. 16, pp. 3071–3074, 2017.

[6] W. Sun, Y. Li, Z. Zhang, and P.-Y. Chen, "Low-profile and wideband microstrip antenna using quasi-periodic aperture and slot-to-CPW transition," *IEEE Trans. Antennas Propag.*, vol. 67, no. 1, pp. 632–637, Jan. 2019.

[7] C. Chiu, B. Lau, and R. Murch, "Bandwidth enhancement technique for broadside tri-modal patch antenna," *IEEE Open J. Antennas Propag.*, vol. 1, pp. 524–533, 2020.

[8] Z. Liu, Y. Zhang, Y. He, and Y. Li, "A compact-size and high-efficiency cage antenna for 2.4-GHz WLAN access points," *IEEE Trans. Antennas Propag.*, vol. 70, no. 12, pp. 12317–12321, Dec. 2022.

[9] R. Ouedraogo, E. Rothwell, A. Diaz, K. Fuchi, and A. Temme, "Miniaturization of patch antennas using a metamaterial-inspired technique," *IEEE Trans. Antennas Propag.*, vol. 60, no. 5, pp. 2175–2182, May 2012.

[10] Y. He and Y. Li, "Dual-polarized microstrip antennas with capacitive via fence for wide beamwidth and high isolation," *IEEE Trans. Antennas Propag.*, vol. 68, no. 7, pp. 5095–5103, Jul. 2020.

[11] Y. Zhang, Z. Xue, and W. Hong, "Planar substrate-integrated end-fire antenna with wide beamwidth for Q-Band applications," *IEEE Antennas Wireless Propag. Lett.*, vol. 16, pp. 1990–1993, 2017.

[12] M. Sun, X. Qing, and Z. Chen, "60-GHz end-fire fan-like antennas with wide beamwidth," *IEEE Trans. Antennas Propag.*, vol. 61, no. 4, pp. 1616–1622, Apr. 2013.

[13] Y. Luo, Q. Chu, and L. Zhu, "A miniaturized wide-beamwidth circularly polarized planar antenna via two pairs of folded dipoles in a square contour," *IEEE Trans. Antennas Propag.*, vol. 63, no. 8, pp. 3753–3759, Aug. 2015.

[14] L. Chang, L. Chen, J. Zhang, and Z. Chen, "A compact wide-band dipole antenna with wide beamwidth," *IEEE Antennas Wireless Propag. Lett.*, vol. 20, pp. 1701–1705, 2021.

[15] C. Shen, W. Lu, and L. Zhu, "Planar self-balanced magnetic dipole antenna with wide beamwidth characteristic," *IEEE Trans. Antennas Propag.*, vol. 67, no. 7, pp. 4860–4865, Jul. 2019.

[16] X. Chen, L. Yang, J. Zhao, and G. Fu, "High-efficiency compact circularly polarized microstrip antenna with wide beamwidth for airborne communication," *IEEE Antennas Wireless Propag. Lett.*, vol. 15, pp. 1518–1521, 2016.

[17] S. Qu, J. Li, and Q. Xue, "Bowtie dipole antenna with wide beamwidth for base station application," *IEEE Antennas Wireless Propag. Lett.*, vol. 6, pp. 293–295, 2007.

[18] L. Wang, Z. Weng, Y. Jiao, W. Zhang, and C. Zhang, "A low-profile broadband circularly polarized microstrip antenna with wide beamwidth," *IEEE Antennas Wireless Propag. Lett.*, vol. 17, pp. 1213–1217, 2018.

[19] M. Boyuan, J. Pan, S. Huang, D. Yang, and Y. Guo, "Wide-beam dielectric resonator antennas based on the fusion of higher-order modes," *IEEE Trans. Antennas Propag.*, vol. 69, no. 12, pp. 8866–8871, Dec. 2021.

[20] S. Mashhadi, Y. Jiao, and J. Chen, "Broadbeam cylindrical dielectric resonator antenna," *IEEE Access*, vol. 7, pp. 112653–112661, 2019.

[21] R. Li, Y. Jiao, Y. Zhang, L. Zhang, and H. Wang, "A DRA with engraved groove and comb-like metal wall for beamwidth enhancement in both E- and H-Planes," *IEEE Antennas Wireless Propag. Lett.*, vol. 20, pp. 543–547, 2021.

[22] J. Yin and L. Zhang, "Design of a dual-polarized magnetoelectric dipole antenna with gain improvement at low elevation angle for a base station," *IEEE Antennas Wireless Propag. Lett.*, vol. 19, pp. 756–760, 2020.

[23] Z. Chen and M. Chia, "Broad-band suspended probe-fed plate antenna with low cross-polarization levels," *IEEE Trans. Antennas Propag.*, vol. 51, no. 2, pp. 345–346, Feb. 2003.

[24] J.-S. Row and Y. H. Chen, "Wideband planar array with broad beamwidth and low cross-polarization," *IEEE Trans. Antennas Propag.*, vol. 63, no. 9, pp. 4161–4165, Sep. 2015.

[25] K.-B. Ng, C. H. Chan, and K.-M. Luk, "Low-cost vertical patch antenna with wide axial-ratio beamwidth for handheld satellite communications terminals," *IEEE Trans. Antennas Propag.*, vol. 63, no. 4, pp. 1417–1424, Apr. 2015.

[26] T. P. Wong and K. M. Luk, "A wide bandwidth and wide beamwidth CDMA/GSM base station antenna array with low backlobe radiation," *IEEE Trans. Veh. Technol.*, vol. 54, no. 3, pp. 903–909, May 2005.

[27] J. Mlynarczyk, "Wide-beam high-efficiency microstrip patch-based antenna for broadband wireless applications," *Microw. Opt. Technol. Lett.*, vol. 53, no. 2, pp. 286–288, Dec. 2010.

[28] C. Su, S. Huang, and C. Lee, "CP microstrip antenna with wide beamwidth for GPS band application," *Electron. Lett.*, vol. 43, no. 20, pp. 1062–1063, Sep. 2007.

[29] S. Noghanian and L. Shafai, "Control of microstrip antenna radiation characteristics by ground plane size and shape," *IEE Proc. Microw. Antennas Propag.*, vol. 145, no. 3, pp. 207–212, Jun. 1998.

[30] M. Khan, M. Sharawi, and R. Mittra, "Microstrip patch antenna miniaturisation techniques: A review," *IET Microw. Antennas Propag.*, vol. 9, no. 9, pp. 913–922, Jun. 2015.

[31] A. K. Shackelford, K.-F. Lee, and K. M. Luk, "Design of small-size wide-bandwidth microstrip-patch antennas," *IEEE Antennas Propag. Mag.*, vol. 45, no. 1, pp. 75–83, Feb. 2003.

[32] K. Gosalia and G. Lazzi, "Reduced size, dual-polarized microstrip patch antenna for wireless communications," *IEEE Trans. Antennas Propag.*, vol. 51, no. 9, pp. 2182–2186, Sep. 2003.

[33] G. Yang, J. Li, D. Wei, S. Zhou, and J. Yang, "Broadening the beamwidth of microstrip antenna by the induced vertical currents," *IET Microw. Antennas Propag.*, vol. 12, no. 2, pp. 190–194, Feb. 2018.

[34] Z. Chen, W. Toh, and X. Qing, "A microstrip patch antenna with broadened beamwidth," *Microw. Opt. Technol. Lett.*, vol. 50, no. 7, pp. 1885–1888, 2008.

[35] X. Chen, P. Qin, Y. Guo, and G. Fu, "Low-profile and wide beamwidth dual-polarized distributed microstrip antenna," *IEEE Access*, vol. 5, pp. 2272–2280, 2017.

[36] Z. Pan, W. Lin, and Q. Chu, "Compact wide-beam circularly-polarized microstrip antenna with a parasitic ring for CNSS application," *IEEE Trans. Antennas Propag.*, vol. 62, no. 5, pp. 2847–2850, May 2014.

[37] G. Yang, J. Li, J. Yang, and S. Zhou, "A wide beamwidth and wide-band magnetoelectric dipole antenna," *IEEE Trans. Antennas Propag.*, vol. 66, no. 12, pp. 6724–6733, Dec. 2018.

[38] Y. He, Y. Li, L. Zhu, and P. Chen, "Miniaturization of omnidirectional cavity antennas using substrate-integrated impedance surfaces," *IEEE Trans. Antennas Propag.*, vol. 69, no. 3, pp. 1728–1733, Mar. 2021.

[39] N. Iizasa, K. Yoshitomi, R. Pokharel, and H. Kanaya, "2 × 2 slot dipole array antenna with CPW for 2.4GHz band," in *Proc. Int. Symp. Antennas Propag. Conf.*, 2014, pp. 603–604.

[40] K. Wong, C. Chen, and W. Li, "Integrated four low-profile shorted patch dual-band WLAN MIMO antennas for mobile device applications," *IEEE Trans. Antennas Propag.*, vol. 69, no. 6, pp. 3566–3571, Jun. 2021.

[41] R. Caso, A. Michel, M. Rodriguez-Pino, and P. Nepa, "Dual-band UHF-RFID/WLAN circularly polarized antenna for portable RFID readers," *IEEE Trans. Antennas Propag.*, vol. 62, no. 5, pp. 2822–2826, May 2014.

[42] H. Kanaya, K. Yamaguchi, Y. Matsushita, T. Kudo, and T. Furuichi, "2.4GHz monopole antenna on flexible substrate for implanting sensor," in *Proc. IEEE Int. Symp. Antennas Propag. USNC/URSI Nat. Radio Sci. Meeting*, 2017, pp. 391–392.